40th Fluid Dynamics Conference and Exhibit
28 June - 1 July 2010, Chicago, Illinois

AIAA 2010-4623

Experimental Study of Near Wake of Micro Vortex Generators in Supersonic Flow

Frank K. Lu,* Adam J. Pierce† and Yusi Shih†
University of Texas at Arlington, Arlington, Texas, 76019

Detailed schlieren and laser lightsheet visualizations of the near wake of micro vortex generator (MVG) revealed large structures that were different from those of the undisturbed turbulent boundary layer. These structures were attributed to the rapid breakdown of the primary trailing vortex pair. The breakdown was thought to arise from a cylindrical Kelvin–Helmholtz-like instability surface. The structures appear to be hairpin or ring-like in nature that showed eruptions into the freestream flow, entraining it.

I. Introduction

MICRO vortex generators (MVGs), whose height is less than the boundary layer thickness, have been lately proposed for mitigating the adverse effects of shock/boundary-layer interactions (SBLIs).[1–17] There is belief that MVGs energize the boundary-layer by vortex entrainment of the freestream although the precise physical mechanisms are still not well understood. This belief is based on surface flow visualizations[6,11,17] which indicate two bright lines downstream of the MVG that apparently disappears after about two MVG lengths downstream (Fig. 1). The disappearance of these lines has been suggested to be due to the vortices lifting off the surface due to upwash from their mutual interaction.[6,11] However, Lu et al.[17] through a detailed study of the topology around an MVG suggest that symmetry breaking at the rear of the MVG leads to a unsteady wake that cannot be captured by surface flow visualization, this technique being regarded as a steady-state one. Moreover, digitally enhanced images[18] show that these two topological lines actually trail further downstream than previously thought. Further, it is not clear from topological considerations that the pair of (primary) vortices are specifically associated with the pair of bright lines. Additionally, based on observations of experimental and numerical surface flow visualizations, topological rules suggest a number of secondary vortex pairs and vortex filament pairs being shed in addition to the primary vortex pair. There is actually a distinct possibility that the bright lines seen in the surface flow visualization are due to a pair of corner (secondary) vortices.

A different downstream flowfield was suggested by Blinde et al.[7] via detailed particle image velocimetry (PIV) mapping. The postulated flowfield, shown in Fig. 2, includes hairpin vortices streaming from the trailing edges of an MVG array, separated by high-speed channels. There are no trailing vortices in this model and this can be interpreted to be due to the breakdown of the trailing vortices but interpreted by others as a lifting from the mutual upwash of the trailing vortex pair. PIV unfortunately was unable to resolve the extremely small vortex filaments.

The mechanism that affects the subsequent shock/boundary-layer interaction, especially separated interactions, also remains the subject of investigation. Thus, the aforementioned model of entrainment of the

*Professor and Director, Aerodynamics Research Center, Department of Mechanical and Aerospace Engineering. Associate Fellow AIAA.
†Graduate Research Assistant, Aerodynamics Research Center, Department of Mechanical and Aerospace Engineering. Student Member AIAA.

freestream by the counter-rotating trailing vortices to energize the boundary layer may be insufficient. It appears that Blinde et al.'s[7] model may point to new physical mechanisms involving impinging hairpin or ring vortices on the shock, thereby disrupting it. The present paper reports flow visualizations which suggest that the trailing vortices downstream of the MVG breaks down. Symmetry breaking[19,20] at the rear of the MVG destabilizes the trailing vortices in what can be considered as a Kelvin–Helmholtz-like instability.[21] This instability is seen to cause the trailing vortices to breakdown rapidly into large vortical structures, identified previously as vortex rings in Li and Liu[15,16] and as hairpin vortices by Blinde et al.[7] Here, the emphasis is on identifying the vortex breakdown mechanism experimentally. This breakdown mechanism can happen rapidly unlike the upwash of a trailing vortex pair in supersonic flow. This latter point is based on observations of the persistence of the signature of trailing vortices shed from protuberances.[22]

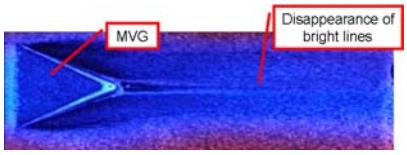

Figure 1. Surface flow visualization showing disappearance of wake signature.[17]

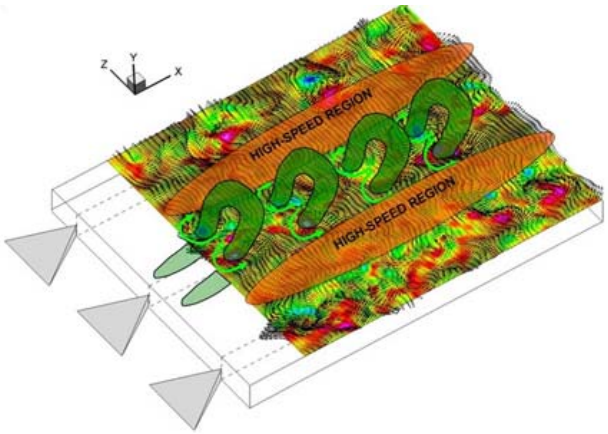

Figure 2. Conceptual sketch of flow downstream of an MVG array, showing the presence of hairpin vortices.[7]

Before examining the supersonic wake of an MVG, it will be useful to briefly review the effect of three-dimensionality on a vortex line perpendicular to the flow direction convecting past a three-dimensional surface mounted obstacle. The vorticity equation, ignoring body forces, can be written as

$$\frac{D\vec{\omega}}{Dt} = (\vec{\omega}\cdot\nabla)\vec{V} - \vec{\omega}(\nabla\cdot\vec{V}) + \frac{1}{\rho^2}\nabla\rho\times\nabla p + \nabla\times\left(\frac{\nabla\cdot\bar{\bar{\tau}}}{\rho}\right) \tag{1}$$

The middle two terms on the RHS of the above equation are absent for incompressible flow while the last term is the viscous dissipation of vorticity, $\bar{\bar{\tau}}$ being the stress tensor. For a two-dimensional flow, the first term on the RHS also vanishes since the velocity vector lies in a plane that is perpendicular to the vorticity vector. Therefore, vorticity is not created and, instead, for a steady, two-dimensional flow, is dissipated.

However, for an obstacle with a finite span mounted on a surface, an incoming, two-dimensional boundary layer that the obstacle is submerged in develops three-dimensionality.[a] Therefore, the first term on the RHS, which is known as the vortex stretching term, is now nonzero due to crossflow terms so that vorticity is created. As has been observed, the vorticity is distributed in such a way that one or more so-called horseshoe vortices wrap around the object, regardless of whether the protuberance is sub-boundary layer in height or taller.[26–28] Such a horseshoe vortex system is extremely persistent since lengthening it increases its vorticity and its well-organized structure even in a turbulent flow. Studies of the downstream evolution of the horseshoe vortex have shown that it eventually breaks down, depending on the Reynolds number

[a]Flows past tall obstacles are known as junction flows. Both protuberance and junction flows are common occurrences, ranging from flows past buildings and other structures, vehicles and circuit boards. Moreover, protuberances of various shapes are used for enhancing heat transfer,[23,24] improving flows when occurring as vortex generators and for tripping boundary layers.[25]

of the flow and the geometry of the obstacle.[29] Compressibility introduces extra terms into the vorticity equation, namely, the second term on the RHS is vortex stretching due to dilatation and the third term is known as the baroclinic torque. Depending on the velocity, density and pressure gradients, these terms can enhance or diminish vorticity. Specifically, for protrusions, such as the MVG in the present study, these gradients increase vorticity due to shocks forming around the obstacle, amongst other causes. The vorticity is mostly confined within the boundary layer, with some arising from the shock envelope around the MVG. The confined vorticity is forced into trailing vortices which stretch, strengthening them. These counter-rotating trailing vortices are regions with high momentum. Sidewash caused by the MVG results in a low momentum, or momentum deficit, region along the centerline of the MVG wake[4,6,7,11,14–16,30] and the high-momentum vortex flows on either side. The shape of the MVG is such that the trailing vortices converge which destabilizes them. Finally, visualizations of a small negative value of λ_2 [31] and an instantaneous numerical schlieren image are shown in Fig. 3.[15] Figure 3(a) shows what are thought to be vortex rings. Analogous, large density structures are visible in the instantaneous schlieren image of Fig. 3(b). These numerical visualizations reveal large structures using different diagnostics than the stereo PIV mapping of Blinde et al.[7]

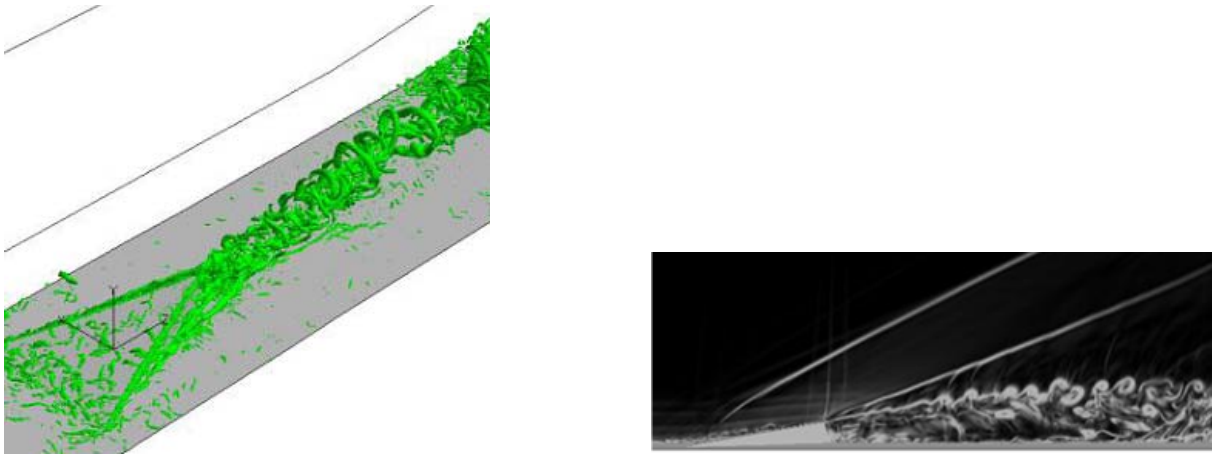

(a) Iso-surface of a small negative value of λ_2.

(b) Instantaneous numerical schlieren.

Figure 3. Visualizations of [15].

Lightsheet visualizations are reported in this paper, including a rarely used local lightsheet technique.[32,33] These visualizations are combined with schlieren visualizations to reveal a highly unsteady wake with large roller structures. There appears to be a distinct difference between these structures and those in the turbulent boundary layer ahead. The present visualizations provide further evidence of a potential vortex breakdown mechanism. The train of either hairpin vortices or vortex rings impinging on the downstream shock is thought to be the key mechanism for disrupting any separated SBLIs downstream which are the subject of future papers.

II. Experiment

The experimental approach is summarized here with details available in [34]. A blowdown wind tunnel operating at a Mach number of 2.47 ± 0.005 was used. The tunnel reached steady-state pressure conditions in 2–3 s.[35] The total pressure was generally kept at 200 ± 6 kPa (29 ± 0.9 psia). The run times of less than

10 s resulted in a total temperature drop of only 1–2 K. The temperature can be considered to be nearly steady and so can the unit Reynolds number be considered at 43 million per m.

The test section was 15.2 cm^2 × 81.28 cm long (6 $in.^2$ × 2.67 ft). It was outfitted with extensive optical access from both sides and from the top. A flat plate, 73 cm long (28.75 in.), with a sharp leading edge of 15 deg was mounted in the test section[36] to develop a boundary layer naturally, with transition occurring within 3 cm (1.2 in.) from the leading edge (Fig. 4). The flat plate was supported in the test section by a sharp-tipped rail on each side. The plate was made in layers. The top layer was made of a number of small, thin plates butted tightly together to form a continuous, flat surface. This modular design allowed for quick configuration changes. A cavity below allowed pressure tubing, transducer wiring and other elements to be placed. The wiring and tubing were channeled to the rear from the side of the test section. Finally, a bottom cover encases the cavity.

Figure 4. Test section showing flat plate. Flow from right to left.

Six MVGs in the form of skewed tetrahedra were distributed evenly across the flat plate such that their leading edges were located 272 mm (10.7 in.) downstream of the leading edge of the flat plate, Fig. 5. The MVGs were 12.95 mm (0.51 in.) long and 1.57 mm (0.062 in.) high. The front of each MVG was 11.7 mm (0.46 in.) wide. The center-to-center spacing between the MVGs was 30.5 mm (1.2 in.). Two styles of MVGs were fabricated based on the designs from [16], with the trailing edge angle of either 45 or 70 deg, labeled as MVG45 and MVG70 respectively. Flow visualizations of either MVG45 and MVG70 are qualitatively very similar. The "nvg431" style based on [37] was also available.

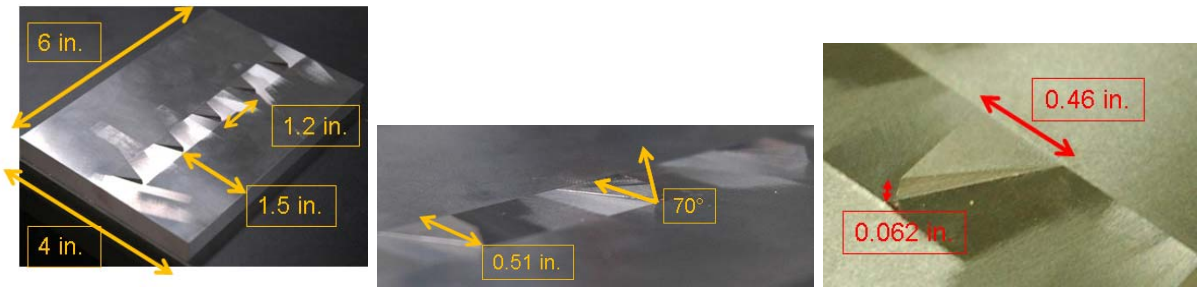

Figure 5. Micro-vortex generator array.

Diagnostics that were applied included schlieren still and video imaging,[38] mean surface pressure measurements downstream of an MVG and at the bisection of two MVGs, surface flow visualization[18] and laser lightsheet visualization using PIV hardware and software. The same setup was used to obtain quantitative velocity data. The schlieren images were obtained by a Nikon D300S camera with a VR 18–200 mm f/3.5–5.6 lens. In still mode, the shutter speed is 1/8000 s and the image consisted of 12.3 megapixels. High-definition video from the camera was at 24 fps and 720 p.

Due to the uniqueness of the lightsheet visualization, some details are provided here. A schematic of the laser lightsheet system is given in Fig. 6. The imaging hardware is a LaVision FlowMaster 3D SPIV system that was installed on a custom-built mounting system. A cylindrical lens with a focal length of −10 mm spreaded a beam of light from a New Wave Research Solo 120 Nd:YAG double-pulsed laser into a 2.5 mm thick sheet. The figure shows the lightsheet incident on the centerline of the flat plate, which also

bisected one of the MVGs. An alternate arrangement had the lightsheet in a crosswise plane, 20.6 (0.81 in.) downstream of the MVG trailing edge.

The lasers were pulsed at 5 Hz with a pulse duration of 0.7 μs. The images were captured by a Flow Master 3S ImagerIntense/ImagePro ICCD camera with 1376 $\times$ 1040 pixel resolution and a 12-bit dynamic range. Other major components of the imaging system included a frame grabber, control electronics and a host computer running the DaVis 7.1 PIV data acquisition and processing software.

A high-pressure seeding system was installed in the plenum chamber of the wind tunnel to spray calcium carbonate particles (Specialty Minerals CalEssence 70) with an average diameter of 0.7 μm. It is thought that this is the first time that calcium carbonate has been used for such a purpose.[39] The suitability of calcium carbonate for seeding high-speed aerodynamics flows and a novel surface treatment to reduce glare are discussed in [34].

In addition to seeding the flow from the plenum chamber, local seeding was accomplished by naturally aspirating acetone from a 2.8 mm (0.11 in.) diameter surface pressure tap 138 mm (5.44 in.) upstream along the centerline of an MVG. A flexible tubing connected the pressure tap to a vial of acetone. Since the pressure in the test section was subatmospheric during a run, the acetone was drawn into the boundary layer via the tap. This local lightsheet visualization technique had been used previously in three-dimensional shock/boundary layer interaction studies.[33,40]

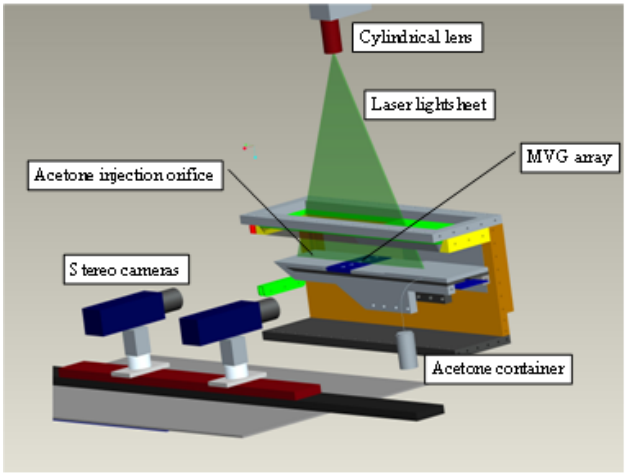

Figure 6. Schematic of laser lightsheet visualization hardware.

III. Results and Discussion

A. Schlieren Visualization

Figure 7 shows schlieren images of the boundary layer past the flat plate and with MVG45. The flow is from right to left as indicated by the large arrow. Due to the high resolution of the cameras, the images show a large number of weak wave reflections which can be traced to joints and surface roughness. Noting that the schlieren technique is sensitive to density gradients, the boundary layer is visible as a bright band with the horizontally mounted knife edge. Figure 7(a) shows a slight irregularity on the boundary-layer edge attributable to a wave from the side wall. Since a schlieren image is integrated along the line of sight, this irregularity appears exaggerated by the dark wave reflection off the boundary layer.

Figure 7(b) shows a curved oblique wave system impinging from the leading edge of the MVG. The curvature is due to the lower Mach number of the flow closer to the surface. The wave system appears to have a λ-foot shape but with the leading and trailing legs inclined close to one another, indicating a weak

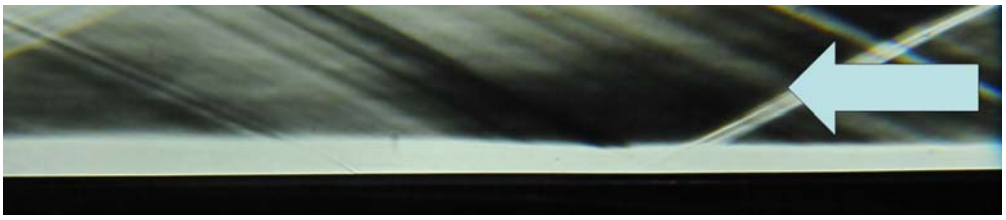

(a) Flat plate.

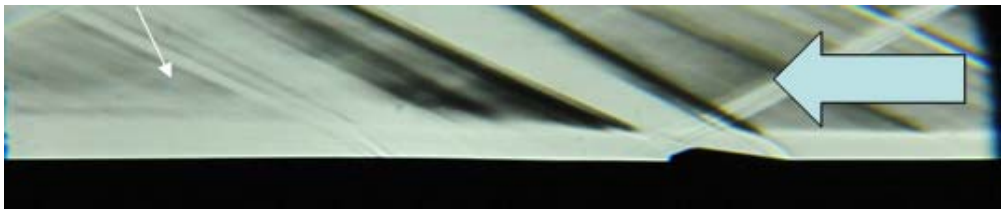

(b) With MVG45.

Figure 7. Schlieren images of Mach 2.47 flow.

separation.[41]

Downstream is a light uniform zone due to the flow past the top of the MVG. This is followed by a dark zone as the flow expands past the trailing edge of the MVG. A more complicated wave system is visible impinging the top of the MVG rear. These waves coalesce just at the edge of the boundary layer to form a single wave. These features are visible in Babinsky et al.[6] as well as in the instantaneous schlieren images of Herges et al.[11]

An important feature in Fig. 7(b) is a broad wispy line downstream of the MVG, this being pointed to by the thin white arrow. This feature is apparently not visible in the instantaneous schlieren images of Herges et al.[11] but is visible and highlighted in Babinsky et al.[6] Babinsky et al. identified this faint line as the outer boundary of a low-momentum region.

B. Lightsheet Visualization

Figure 8 presents global laser lightsheet visualization along the centerline of MVG70. The flat plate is outlined in the image for clarity. Due to the multiple MVGs and the camera perspective, blurred images of the other MVGs outside of the camera's depth of focus are also visible in Fig. 8. The figure shows large structures in the undisturbed boundary layer as faint dark objects inclined downstream. In the near wake of the MVG, however, the visualization shows a distinct train of large billowing structures that appears to be different from those upstream. The increased prominence of the large structures downstream of the MVG can be compared with the numerical schlieren results of Fig. 3(b).

Note that since the boundary layer is devoid of particles in global lightsheet visualization, boundary layer structures tend to appear as dark images. Further revelation of the influence of the MVG on the boundary layer is obtained using local laser lightsheet visualization where the boundary layer is seeded by a port located directly upstream of the MVG (see Section II). Figure 9 shows local lightsheet visualizations of the flat plate and when an MVG is mounted on it. The change in the large structures due to the presence of the MVG is obvious. Figure 9(b) is able to show smaller structures that are not visible in Fig. 8.

It is also worthwhile to compare these images with those of Fig. 7. It appears that the faint line identified in Fig. 7(b) may be associated with the intermittent outer boundary of the large downstream structures, absent in the boundary layer over a flat plate. This intermittent outer boundary appears as a faint feature in the schlieren image since it does not spread over the entire span of the flat plate, noting that schlieren imaging integrates all density gradients along its field of view. Babinsky et al.[6] remarked that the faint line as indicated in Fig. 7(b) is the upper boundary of a low-momentum region. The present visualizations shown in Fig. 7(b) indicates a broad band instead of a thin line. Thus, the present visualizations suggest more specifically that this faint broad band marks the intermittent interface between large structures in the MVG wake. The visualizations also suggest that time-resolved schlieren may not be able to reveal such a band whereas an averaging procedure can.

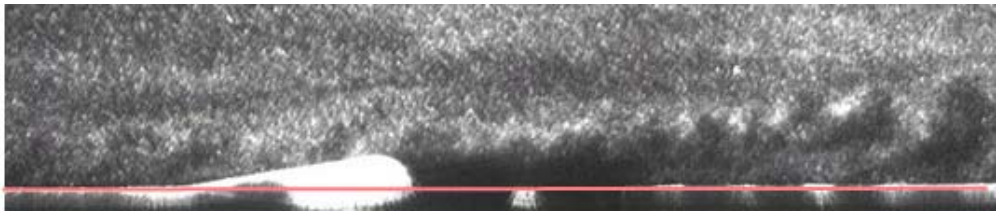

Figure 8. Global lightsheet visualization of MVG70 with lightsheet aligned along MVG axis.

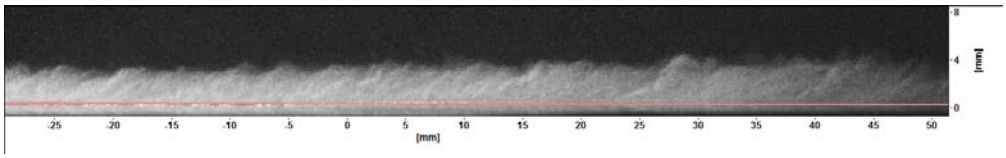

(a) Flat plate

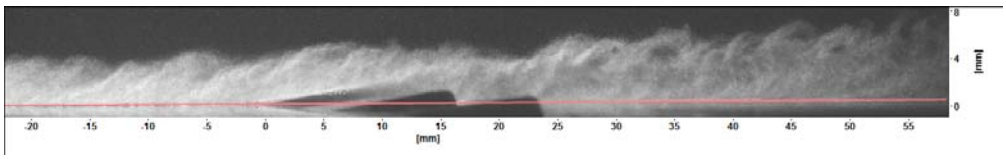

(b) With MVG70

Figure 9. Comparison between local lightsheet visualization of flat plate and MVG70.

Kleine[42] remarked that videographic imaging allows small or obscure features to be revealed that may otherwise be thought to be "noise" or other flaws. Following this argument, even if the images are not time resolved, video images are expected to help in understanding the MVG wake. Thus, Figs. 10 and 11 show consecutive frames from local lightsheet visualizations of the flat plate and with MVG70 respectively. Despite the low framing rate of the camera, two important observations can be made. First, as in the previous global visualization, there is a distinct difference in the shape of the large turbulent structures over the bare flat plate and downstream of an MVG. Secondly, there are features around the MVG that appear relatively steady and others that show a highly intermittent edge. The visualizations show that the flowfield nearest the MVG, namely, the primary vortex is turbulent but does not show evidence of large-scale intermittency. Further downstream, it appears that the primary vortex breaks down to form the large roller structures

which exhibit severe intermittency, identified by Li and Liu[15] as ring vortices and Blinde et al.[7] as hairpin vortices.

For further clarification, portions of Fig. 11(j) are enlarged and shown in Fig. 12. The difference between the large structures of the incoming boundary layer as shown in Fig. 12(a) compared to downstream of the MVG as shown in Fig. 12(c) is clearly evident. In the latter, large swirls of boundary layer fluid are seen to erupt into the free stream. It is fair to conclude, at least along the centerplane of the MVG wake, that there is significant entrainment of the freestream fluid and a high level of intermittency.

Further, Fig. 12(b) shows a sharp inclined demarcation between the incoming boundary layer and the MVG wake. The demarcation appears to be relatively steady with some flutter between frames. This demarcation is thought to indicate the primary vortex shed off the MVG side.[17] Note that the lightsheet is located at the centerplane while the primary vortex is slightly off the centerplane. Therefore, less light is scattered off the primary vortex and thus it appears a little darker in all the frames of Fig. 11. Figure 12(b) shows the rapid breakdown of the primary vortex at about two lengths behind the MVG trailing edge. This is consistent with surface flow visualizations which shows the disappearance of two bright lines.[6,11,17] (Note that digitally enhanced images show that these two lines extend much further downstream.[18])

C. Further Discussion

Babinsky et al.[6] and Herges et al.[11] thought that the disappearance of the bright lines is due to the two primary vortices being lifted from the surface due to mutual upwash. However, based on topological considerations, the two bright lines in surface flow visualization are not associated with the primary vortex pair but may be attributed to two secondary vortices along the corner of the MVG with the flat plate that originate from the leading-edge tips of the MVG. These vortices, as they clash behind the MVG, are likely to be unsteady due to symmetry breaking and break down.

However, it is the break down of the primary vortex pair that is important here due to their relatively large size and the outcome on downstream interactions. The breakdown of the primary vortex pair may be due to the presence of an inflection surface of the velocity profile in the MVG wake, the so-called momentum deficit. This inflection surface is somewhat circular[15] and is analogous to the inflection point in plane shear flow. Thus, this type of instability is labeled Kelvin–Helmholtz-like[21] and observed in the wakes of wall-mounted obstacles at low speeds by various authors.[29,43–45] Mason and Morton[43] suggested that inner vortices, which may be the primary vortices of MVGs, are dominant and, even though they become unstable and break up, the presence of these vortices is noticeable far downstream.

Velte et al.[46] observed the presence of embedded longitudinal vortices shed from sub-boundary layer vanes and discussed how vorticity rearranges the axial momentum distribution to the crosswise direction. Lögdberg et al.'s[47] visualizations showed a pair of turbulent vortical structures being convected downstream. Their hotwire measurements indicated the presence of strong counter-rotating vortices emanating from the MVGs but no evidence of unsteadiness was offered. These authors suggested the presence of a "hooklike" vortex core motion persisting as far as 200 vortex heights downstream.

Other studies have provided evidence that the flow downstream of an MVG array is unsteady.[48] Angele and Grewe[48] suggested that the unsteadiness contributes to maximum Reynolds stresses around the mean vortex centers which should not be the case if the vortices were steady. Duriez et al.[49] suggested that steady spatial forcing at different wavelengths produces a self-sustaining process between the streamwise velocity streaks in a turbulent boundary layer and the streamwise vortices generated by an MVG array.

The circular upwash with momentum deficit has been observed in the wakes of surface-mounted obstacles at low and high speeds. Present evidence of this feature is provided indirectly by visualizations where the lightsheet is located in a crosswise plane 20.6 mm (0.81 in.) downstream of the MVG trailing edge. A few sequential frames at 15 Hz are shown in Fig. 13(a)–13(d). These individual frames show an unsteady roundish blob of light scattered by the acetone droplets. This local lightsheet visualization technique was deliberately used to highlight the flow within the boundary layer, as contrasted against the spanwise global lightsheet visualization of Bur et al.[8] In the latter technique, the lack of seeding in the boundary layer

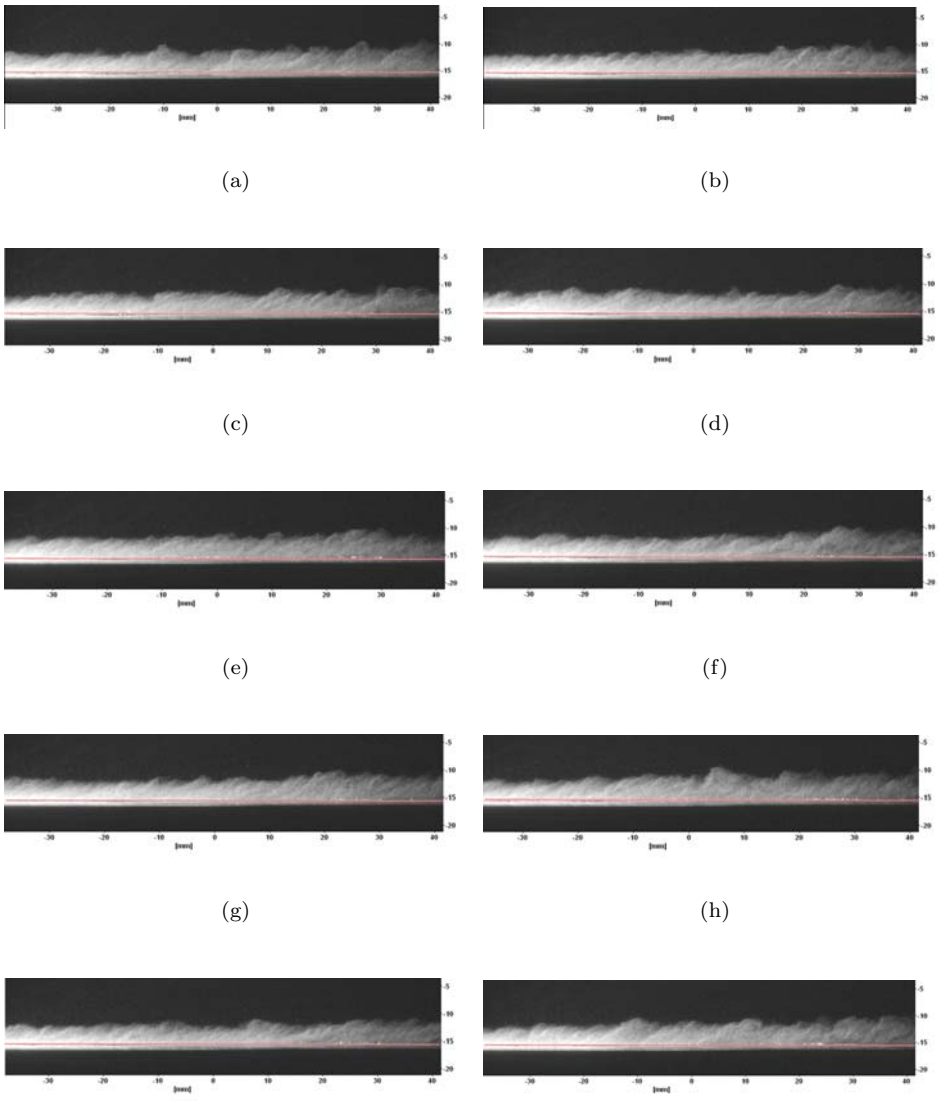

(a) (b)

(c) (d)

(e) (f)

(g) (h)

(i) (j)

Figure 10. Sequence of frames at 15 Hz from local laser lightsheet visualization of bare flat plate.

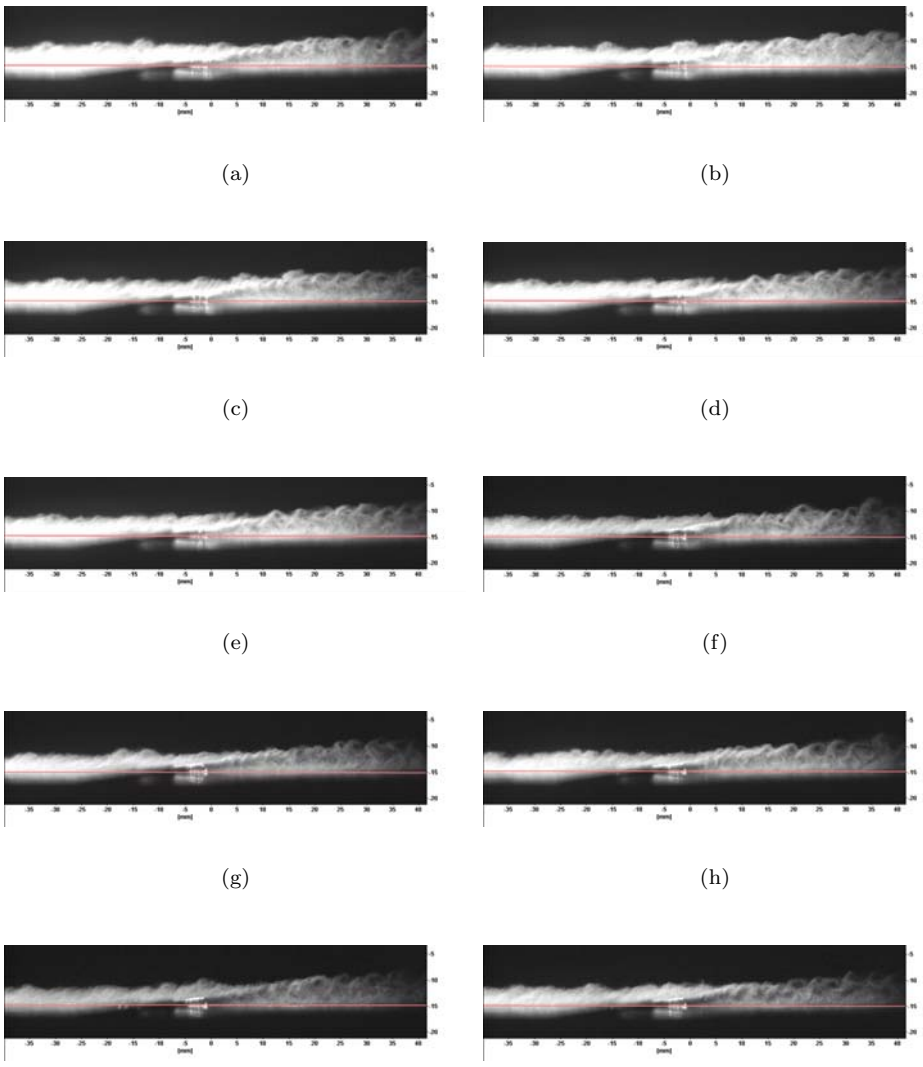

(a) (b)

(c) (d)

(e) (f)

(g) (h)

(i) (j)

Figure 11. Sequence of frames at 15 Hz from local laser lightsheet visualization of MVG.

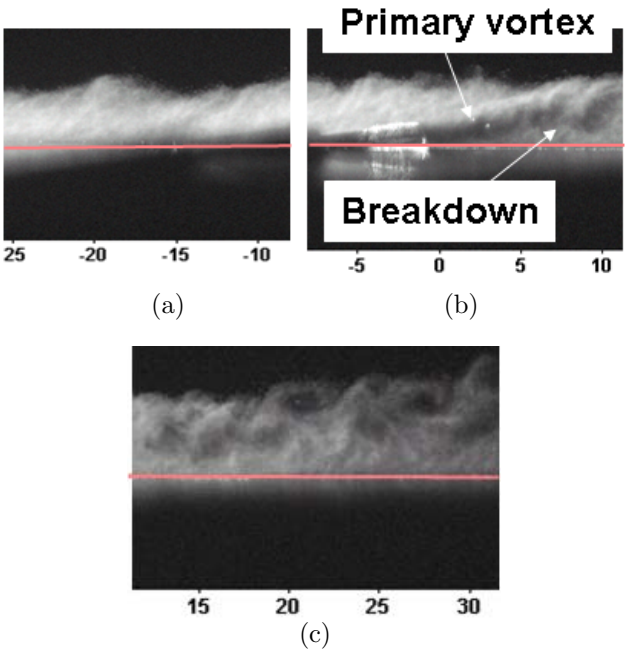

Figure 12. Enlargements of Fig. 11(j).

resulted in these regions being dimly lit.

The rms of the light intensity of 118 images is shown in Fig. 13(g) to highlight the roundish structure. The figure reveals that there is a structure with an unsteady rim. This unsteadiness can be interpreted to be due to the convection of the large structures arising from the trailing vortex breakdown. It is not entirely clear in the visualization whether these structures are haipin or ring shaped, although this distinction may not be a critical one on how these vortical structures interact with a downstream separated zone.

IV. Conclusions

Detailed lightsheet visualizations of the near wake of an MVG reveal the presence of large roller structures that were previously identified as hairpin or ring vortices. These structures show a high level of intermittency. These structures are considered to arise from the rapid break down of the primary vortex pair due to a cylindrical Kelvin–Helmholtz-like instability surface.

Acknowledgments

The authors gratefully acknowledge funding for this work via AFOSR Grant No. FA9550-08-1-0201 monitored by Dr. John Schmisseur. The authors thank the assistance of Rod Duke and David Whaley with the experiments. David Whaley was supported by a High School Research Internship under a Texas Youth in Technology grant from the Texas Workforce Commission, administered by Dr. J. Carter M. Tiernan. The authors also acknowledge Richard R. Mitchell for designing the high-pressure seed injection system. Finally, the authors appreciate discussions with Prof. C. Liu and Dr. Q. Li.

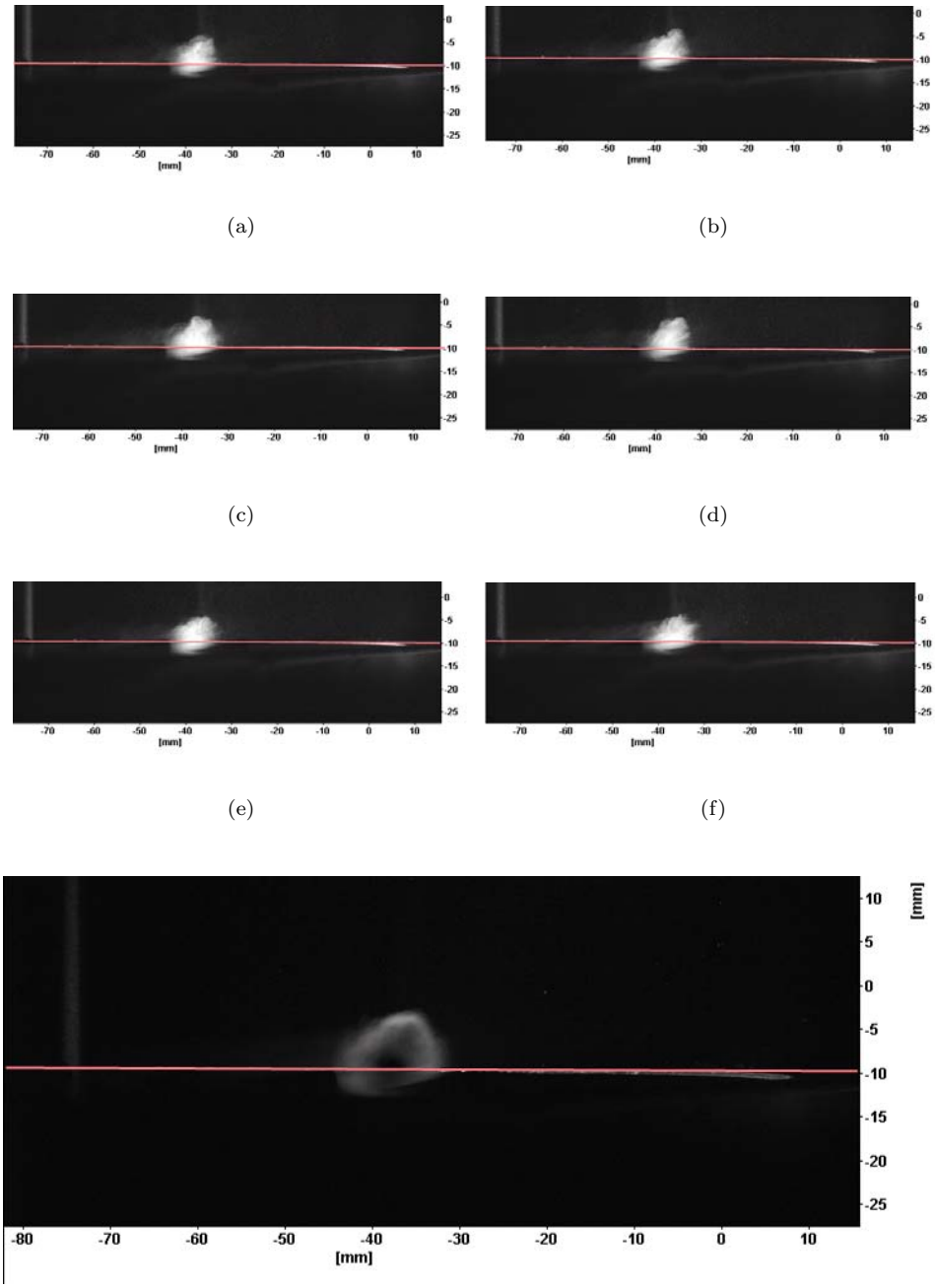

(a) (b)

(c) (d)

(e) (f)

(g) RMS of 118 frames.

Figure 13. Spanwise, local laser light sheet visualization of MVG45.

References

[1]Babinsky, H., Makinson, N. J., and Morgan, C. E., "Micro-Vortex Generator Flow Control for Supersonic Engine Inlets," AIAA Paper 2007–2007, 2007.

[2]Holden, H. and Babinsky, H., "Effect of Microvortex Generators on Separate Normal Shock/Boundary Layer Interactions," *Journal of Aircraft*, Vol. 44, No. 1, 2007, pp. 89–96.

[3]Shinn, A. F., Vanka, S. P., Mani, M., Dorgan, A., and Michal, T., "Application of BCFD Unstructured Grid Solver to Simulation of Micro-Ramp Control of Shock/Boundary Layer Interactions," AIAA Paper 2007–3914, 2007.

[4]Babinsky, H. and Ogawa, H., "SBLI Control for Wings and Inlets," *Shock Waves*, Vol. 18, No. 2, 2008, pp. 89–96.

[5]Anderson, B. H., Mace, J. L., and Mani, M., "Active 'Fail Safe' Micro-Array Flow Control For Advanced Embedded Propulsion Systems," AIAA Paper 2009–0920, 2009.

[6]Babinsky, H., Li, Y., and Pitt Ford, C. W., "Microramp Control of Supersonic Oblique Shock-Wave/Boundary-Layer Interactions," *AIAA Journal*, Vol. 47, No. 3, 2009, pp. 668–675.

[7]Blinde, P. L., Humble, R. A., van Oudheusden, B. W., and Scarano, F., "Effects of Micro-Ramps on a Shock Wave/Turbulent Boundary Layer Interaction," *Shock Waves*, Vol. 19, No. 6, 2009, pp. 507–520.

[8]Bur, R., Coponet, D., and Carpels, Y., "Separation Control by Vortex Generator Devices in a Transonic Channel Flow," *Shock Waves*, Vol. 19, No. 6, 2009, pp. 521–530.

[9]Domel, N. D., Baruzzini, D., and Miller, D. N., "CFD Results for Shock-Boundary Layer Flow Control with Micro-Ramps at Various Grid Densities," AIAA Paper 2009–4016, 2009.

[10]Galbraith, M. C., Orkwis, P. D., and Benek, J. A., "Multi-Row Micro-Ramp Actuators for Shock Wave Boundary-Layer In-teraction Control," AIAA Paper 2009–0321, 2009.

[11]Anderson, T., Kroeker, E., Elliott, G., and Dutton, J., "Micro-Ramp Flow Control of Normal Shock/Boundary Layer Interactions," AIAA Paper 2009–0920, 2009.

[12]Lee, S., Loth, E., Georgiadis, N. J., and DeBonis, J. R., "Effect of Mach Number on Flow Past Micro-Ramps," AIAA Paper 2009–4181, 2009.

[13]Rybalko, M., Loth, E., Chima, R. V., Hirt, S. M., and DeBonis, J. R., "Micro-Ramps for External Compression Low-Boom Inlets," AIAA Paper 2009–4206, 2009.

[14]Lee, S., Goettke, M. K., Loth, E., Tinapple, J., and Benek, J., "Microramps Upstream of an Oblique-Shock/Boundary-Layer Interaction," *AIAA Journal*, Vol. 48, No. 1, 2010, pp. 104–118.

[15]Li, Q. and Liu, C., "LES for Supersonic Ramp Control Flow Using MVG at $M = 2.5$ and $Re_\theta = 1440$," AIAA Paper 2010–0592, 2010.

[16]Li, Q. and Liu, C., "Numerical Investigation on the Effects of the Declining Angle of the Trailing Edge of MVG," AIAA Paper 2010–0714, 2010.

[17]Lu, F. K., Pierce, A. J., Shih, Y., Liu, C., and Li, Q., "Experimental and Numerical Study of Flow Topology Past Micro Vortex Generators," AIAA Paper 2008–4463, 2010.

[18]Pierce, A. J., Lu, F. K., Bryant, D. S., and Shih, Y., "New Developments in Surface Oil Flow Visualization," AIAA Paper 2010–4353, 2010.

[19]Crawford, J. D. and Knobloch, E., "Symmetry and Symmetry-Breaking Bifurcations in Fluid Dynamics," *Annual Review of Fluid Mechanics*, Vol. 23, 1991, pp. 341–387.

[20]Bridges, D. H., "Toward a Theoretical Description of Vortex Wake Asymmetry," *Progress in Aerospace Sciences*, Vol. 46, No. 2–3, 2010, pp. 62–80.

[21]Lim, T. T., "On the Role of Kelvin–Helmholtz-Like Instability in the Formation of Turbulent Vortex Rings," *Fluid Dynamics Research*, Vol. 21, No. 1, 1997, pp. 47–56.

[22]Sedney, R., "A Survey of the Effects of Small Protuberances on Boundary-Layer Flows," *AIAA Journal*, Vol. 11, No. 6, 1973, pp. 782–792.

[23]Jacobi, A. M. and Shah, R. K., "Heat Transfer Surface Enhancement Through the Use of Longitudinal Vortices: A Review of Recent Progress," *Experimental Thermal and Fluid Science*, Vol. 11, 1995, pp. 295–309.

[24]Chyu, M. K. and Natarajan, V., "Heat Transfer on the Base Surface of Three-Dimensional Protruding Elements," *International Journal of Heat and Mass Transfer*, Vol. 39, 1996, pp. 2925–2935.

[25]Klebanoff, P. S., Cleveland, W. G., and Tidstrom, K. D., "On the Evolution of a Turbulent Boundary-Layer Induced by a Three-Dimensional Roughness Element," *Journal of Fluid Mechanics*, Vol. 237, 1992, pp. 101–187.

[26]Baker, C. J., "The Laminar Horseshoe Vortex," *Journal of Fluid Mechanics*, Vol. 95, 1979, pp. 347–367.

[27]Baker, C. J., "The Turbulent Horseshoe Vortex," *Journal of Wind Engineering and Industrial Aerodynamics*, Vol. 6, 1980, pp. 9–23.

[28]Simpson, R. L., "Junction Flows," *Annual Review of Fluid Mechanics*, Vol. 33, 2001, pp. 415–443.

[29]Sau, A., Hwang, R. R., Sheu, T. W., and Wang, W. C., "Interaction of Trailing Vortices in the Wake of a Wall-Mounted Rectangular Cylinder," *Physical Review E*, Vol. 68, No. 5, 2003, Article No. 056303.

[30]Ghosh, S., Choi, J.-I., and Edwards, J. R., "RANS and Hybrid LES/RANS Simulation of the Effects of Micro Vortex Generators Using Immersed Boundary Methods," AIAA Paper 2008–3728, 2008.

[31]Jiang, M., Machiraju, R., and Thompson, D. S., "Detection and Visualization of Vortices," *Visualization Handbook*, edited by C. R. Johnson and C. D. Hansen, Elsevier, 2005, pp. 295–309.

[32]Settles, G. S. and Teng, H. Y., "Flow Visualization Methods for Separated 3-Dimensional Shock-Wave Turbulent Boundary-Layer Interactions," *AIAA Journal*, Vol. 21, No. 3, 1983, pp. 390–397.

[33]Settles, G. S., "Modern Developments in Flow Visualization," *AIAA Journal*, Vol. 24, No. 8, 1986, pp. 1313–1323.

[34]Pierce, A. J., *Experimental Study of Micro-Vortex Generators at Mach 2.5*, MSAE thesis, University of Texas at Arlington, 2010.

[35]Braun, E. M., Lu, F. K., Mitchell, R. R., Wilson, D. R., and Dutton, J. C., "Supersonic Blowdown Wind Tunnel Control Using LabVIEW," AIAA Paper 2008–0852, 2008.

[36]Mitchell, R. R. and Lu, F. K., "Development of a Supersonic Aerodynamic Test Section using Computational Modeling," AIAA Paper 2009–3573, 2009.

[37]Anderson, B. H., Tinapple, J., and Sorber, L., "Optimal Control of Shock Wave Turbulent Boundary Layer Interactions Using Micro-Array Actuation," AIAA Paper 2006–3197, 2006.

[38]Pierce, A. J. and Lu, F. K., "Laser Alignment Method for Portable Schlieren System," AIAA Paper 2009–3574, 2009.

[39]Raffel, M., Willert, C., Wereley, S., and Kompenhans, J., *Particle Image Velocimetry: A Practical Guide*, Springer, Berlin, 2nd ed., 2007.

[40]Settles, G. S. and Lu, F. K., "Conical Similarity of Shock/Boundary-Layer Interactions Generated by Swept and Unswept Fins," *AIAA Journal*, Vol. 23, No. 7, 1985, pp. 1021–1027.

[41]Settles, G. S., Bogdonoff, S. M., and Vas, I. E., "Incipient Separation of a Supersonic Turbulent Boundary Layer at High Reynolds Numbers," *AIAA Journal*, Vol. 14, 1976, pp. 50–56.

[42]Kleine, H., "Filming the Invisible–Time-Resolved Visualization of Compressible Flows," *European Physical Journal—Special Topics*, Vol. 182, 2010, (to appear).

[43]Mason, P. J. and Morton, B. R., "Trailing Vortices in the Wakes of Surface-Mounted Obstacles," *Journal of Fluid Mechanics*, Vol. 175, 1987, pp. 247–293.

[44]Hwang, J. Y. and Yang, K. S., "Numerical Study of Vortical Structures Around a Wall-Mounted Cubic Obstacle in Channel Flow," *Physics of Fluids*, Vol. 16, 2004, pp. 2382–2394.

[45]Yakhot, A., Anor, A., Liu, H. P., and Nikitin, N., "Direct Numerical Simulation of Turbulent Flow Around a Wall-Mounted Cube: Spatio-Temporal Evolution of Large-Scale Vortices," *Journal of Fluid Mechanics*, Vol. 566, 2006, pp. 1–9.

[46]Velte, C. M., Hansen, M. O. L., and Okulov, V. L., "Helical Structure of Longitudinal Vortices Embedded in Turbulent Wall-Bounded Flow," *Journal of Fluid Mechanics*, Vol. 619, 2009, pp. 167–177.

[47]Lögdberg, O., Fransson, J. H., and Alfredsson, P. H., "Streamwise Evolution of Longitudinal Vortices in a Turbulent Boundary Layer," *Journal of Fluid Mechanics*, Vol. 623, 2009, pp. 27–58.

[48]Angele, K. P. and Grewe, F., "Instantaneous Behavior of Streamwise Vortices for Turbulent Boundary Layer Separation Control," *Journal of Fluids Engineering*, Vol. 129, 20006, 226–235.

[49]Duriez, T., Aider, J.-L., and Wesfreid, J. E., "Self-Sustaining Process through Streak Generation in a Flat-Plate Boundary Layer," *Physical Review Letters*, Vol. 103, 2009, Article No. 144502.